Optimization of Er, Yb:YCOB for CW Laser Operation

Phillip A. Burns, *Member, IEEE*, Judith M. Dawes, Peter Dekker, James A. Piper, Huaidong Jiang, and Jiyang Wang

***Abstract*—The erbium and ytterbium ion concentrations in the host yttrium calcium oxaborate have been optimized for diode pumped continuous-wave (CW) laser operation using spectroscopic measurements, modeling of energy transfer and population rate equation analysis, resulting in 270 mW of CW output from a diode-pumped Er,Yb:YCOB laser.**

***Index Terms*—Diode-pumped solid-state laser, quasi-three-level laser.**

I. Introduction

ERBIUM-DOPED laser materials are widely used for the generation of near infrared light at 1.5-μm with potential applications including laser-range-finding, remote sensing, medicine, and detection of atmospheric phenomena. However, erbium-doped crystals suffer reduced efficiency from poor pump absorption and excited state absorption. Sensitizer ions such as ytterbium are added to the crystal to offer improved pump absorption, and hence, laser operation, via energy transfer to the erbium ions [3]–[8].

Here, energy-transfer mechanisms in Yb^{3+}–Er^{3+} doped $YCa_4O(BO_3)_3$ (YCOB) laser crystals are investigated. Energy transfer rates in various hosts are compared and a rate-equation analysis is undertaken to determine optimum parameters for Er,Yb:YCOB. Efficient continuous-wave (CW) TEM_{00} laser operation on the 1.5-μm ($^4I_{13/2}$-$^4I_{15/2}$) transition of Er,Yb:YCOB with over 250 mW of output from a hemispherical laser cavity, and 150 mW of output from a plane-plane cavity with power variation of $\sim 1\%$, are demonstrated.

II. Microscopic Analysis of Energy Transfer

Pioneering work by Förster [9] and Dexter [10] developed the theory of resonant energy transfer between two allowed transitions. The Er activator can luminesce after energy transfer from the absorbing Yb sensitizer. The resonant energy transfer rate via dipole–dipole interactions is strongly dependent on the interaction distance R_{sa}. The ion interaction strength can be determined from experimental measurements of oscillator strengths, absorption coefficients and decay times. The rate of energy transfer W_{sa} for dipole–dipole coupling between ions [10] independent of the ion concentrations is given by

$$W_{\mathrm{sa}} = \frac{c_{\mathrm{sa}}}{R_{\mathrm{sa}}^6} \tag{1}$$

$$c_{\mathrm{sa}} = \frac{3}{4\pi} A_s Q_{\mathrm{abs}} \int \frac{F_s(\omega) f_a(\omega)}{\omega^4} d\omega \tag{2}$$

where $A_s = 1/\tau_s$ is the radiative transition rate of the sensitizer and Q_{abs} is the integrated absorption cross section defined as $\int \sigma^{\mathrm{abs}}(\omega) d\omega$. c_{sa} is the microscopic interaction parameter which characterizes the strength of the interaction between the emission of the sensitizer $F_s(\omega)$ and the absorption of the activator $f_a(\omega)$. The integrals of $F_s(\omega)$ and $f_a(\omega)$ have units of $[\mathrm{cm}^2 \cdot \mathrm{s}^{-1}]$ giving c_{sa} units of $[\mathrm{cm}^6 \cdot \mathrm{s}^{-1}]$.

A. Migration-Enhanced Energy Transfer

The above theory should be modified to include effects due to a high concentration of sensitizer ions in the host material. As the distance between the ions decreases, the probability that the energy residing on an excited ion migrates among its neighbors increases. The energy is then trapped on the activator for example, because the activator ion exhibits a secondary energy level close to the transfer level. The electron decays quickly to this secondary level via phonon relaxation, thus reducing the possibility of a back-transfer interaction. There are two approaches to analyze energy migration, one based on a random walk model (the hopping model [11]), and the other based on a diffusion approach. Migration via the hopping model generally occurs over large distances (tens of angstroms), i.e., in weakly doped host materials. With diffusion, the excitation can transfer to the activator more efficiently by diffusing through the lattice to interact at shorter distances, rather than directly over a large distance.

The diffusion of energy among excited sensitizers was modeled by Bloembergen [12]. If the diffusion rate is faster than the sensitizer-activator transfer rate, then the sensitizer-activator interaction occurs over roughly the same distance across the entire ensemble of impurity ions. Taking this into consideration, Tkachuk [13] derived the energy-transfer rate in this "migration-limited" regime

$$W_{\mathrm{sa}} = \frac{4\pi^3\sqrt{2\pi}}{9} N_s N_a \sqrt{c_{\mathrm{ss}}^{\mathrm{mig}} c_{\mathrm{sa}}} \tag{3}$$

where N_s and N_a are the concentrations of the sensitizer and the activator impurity ions, c_{sa} is the microscopic interaction parameter, and $c_{\mathrm{ss}}^{\mathrm{mig}}$ is the migration interaction parameter. $c_{\mathrm{ss}}^{\mathrm{mig}}$ is found using (2) by considering the sensitizer ion to be both sensitizer and activator, assuming that $c_{\mathrm{ss}}^{\mathrm{mig}} \gg c_{\mathrm{sa}}$.

Manuscript received March 11, 2004; revised June 16, 2004.

P. A. Burns was with the Centre for Lasers and Applications, Department of Physics, Sydney NSW 2109, Australia. He is now with Shelston IP, Sydney, NSW 2109, Australia.

J. M. Dawes, P. Dekker, J. A. Piper, and H. Jiang are with the Centre for Lasers and Applications, Department of Physics, Sydney, NSW 2109, Australia.

J. Wang was with Shandong University, Jinan City 250100, China. He is now with the Department of Physics, National University of Singapore, Singapore.

Digital Object Identifier 10.1109/JQE.2004.834935

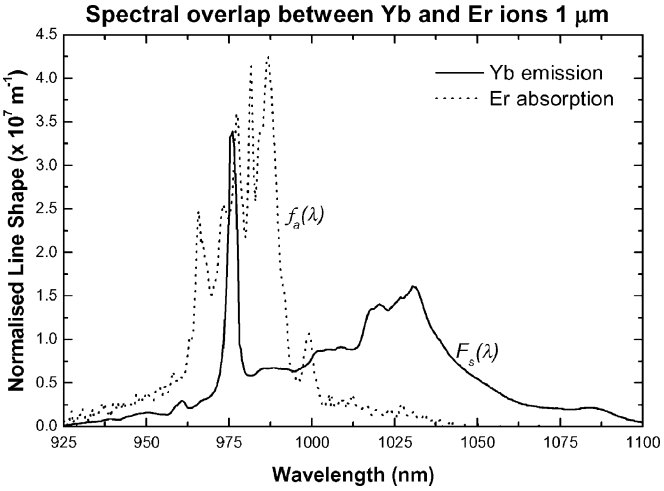

Fig. 1. Spectral overlap between the emission of the Yb^{3+} sensitizer ions, $F_s(\lambda)$, and the absorption of the Er^{3+} activator ions, $f_a(\lambda)$.

III. Energy-Transfer Parameters of Er,Yb:YCOB

Energy-transfer from the Yb^{3+} to the Er^{3+} ions in the YCOB host is strongly favored. There is a good overlap between the Yb^{3+} emission and the Er^{3+} absorption at about 1 μm, which is essential for efficient resonant energy transfer. (Fig. 1 shows an overlay of the two normalized spectra.) The phonon energy distribution of the YCOB host also supports efficient energy transfer. Raman spectra of the YCOB crystal show the maximum phonon energy available is $\sim$ 1550 cm^{-1}. This is significantly higher than the effective phonon energy for other erbium/ytterbium hosts [14], [15]. Deactivation of the Er^{3+} excitation to the upper laser level is, thus, rapid (12.6 μs) and is much quicker than the decay of the Yb^{3+} $^2F_{5/2}$ manifold (2.6 ms), ensuring the efficiency of the Yb^{3+} to Er^{3+} energy transfer.

Other favorable aspects of the YCOB host for laser operation are the large crystal-field splitting and the large emission bandwidth greater than 75 nm. The effect of thelarge crystal field splitting is to reduce the Boltzmann population in the upper energy levels of the manifold and increase the efficiency of the three-level laser transition. This property, along with good mechanical (e.g, hygroscopicity) and thermal (e.g., thermal conductivity and expansion) properties contributes to the effectiveness of the crystal as a laser host.

To determine the energy-transfer parameters of the Er,Yb:YCOB crystal, a sample crystal was grown by the Czochralski method with 20 at.% Yb^{3+} ions and 2 at.% Er^{3+} impurity ions [16]. Since this Yb^{3+} concentration is quite high, we assumed the diffusion model of energy migration among Yb^{3+} ions and (3) was used to calculate the energy-transfer rate.

Spectroscopic analysis of the Er,Yb:YCOB crystal [17] enabled the relevant energy-transfer parameters to be calculated as listed in Table I for YCOB and other Er^{3+}/Yb^{3+} laser host materials. The assumed dopant concentrations in Er,Yb:YCOB were $N_{\rm Yb} = N_s = 2$ at. % and $N_{\rm Er} = N_a = 2$ at. %. The micro-parameter for migration between Yb^{3+} ions was calculated from the overlap between the absorption and emission of the Yb^{3+} ions using (2). The other parameters used were the integrated absorption coefficient $Q_{\rm abs} = 1.7601 \times 10^{-17}$ cm, and the radiative transition rate $A_s = 396.2\ {\rm s}^{-1}$. For the Yb^{3+}-Er^{3+} micro-parameter calculation, the normalized absorption and emission spectra (shown in Fig. 1) were integrated to give $Q_{\rm abs} = 3.8409 \times 10^{-18}$ cm and $c_{\rm sa} = 2.7 \times 10^{-39}\ {\rm cm}^6{\rm s}^{-1}$. The energy-transfer rate from (3) is significantly higher than that for hosts such as Er,Yb:YAG and Er,Yb:YLF. The critical radius $R_{\rm sa}$ for YCOB crystals was calculated as 7.7 Å, which is about half the value for phosphate glass listed in Table I [1].

Since no significant back-transfer of energy occurs in the YCOB host, we assume that upconversion from the upper state laser manifold ($^4I_{13/2}$ in Er) is the main loss channel for ions once they reach this manifold. The upconversion parameter has been calculated by fitting the decay from this manifold to (A4) given in the Appendix. The upconversion parameter $W_{\rm UC}$ was varied to match the decay data from experimental measurements. (See Fig. 2 for a crystal with 2 at.% Er^{3+}.) The upconversion parameter was calculated to be $W_{\rm UC} = (1.30 \pm 0.4) \times 10^{-17}\ {\rm s}^{-1}$.

Since the energy-transfer rate is highly dependent on the rare-earth concentrations, and particularly on the ratio of the Yb^{3+} to Er^{3+} ions, a concentration-independent parameter (after [4]) can be used to compare host materials directly. Table I shows that the concentration-independent energy-transfer rate in the YCOB host is much greater than that for other hosts.

We checked the validity of the diffusion model for our case. Yokota and Tanimoto [18] have developed a time-dependent solution of the diffusion (4) that can be used to fit the decay of the Yb^{3+} sensitizer ion to an equation of the form

$$n(t) = n_o e^{-1/\tau} \cdot \exp\left[-\frac{4}{3}\pi^{3/2} N_a \sqrt{c_{\rm sa} \cdot t}\left\{\frac{1+8.47x+15.5x^2}{1+8.74x}\right\}^{3/4}\right] \quad (4)$$

where $n(t)$ is the excitation population at time t, and $x = DC_{\rm sa}^{-1/3}t^{2/3}$.

Fig. 3 shows that the fit of the 1-μm Yb^{3+} fluorescence to (6) assuming $D = 1.0 \times 10^{-10}\ {\rm cm}^2/{\rm s}$, offers excellent agreement with the experimental data. In contrast, the hopping model [11] predicts that the sensitizer decays with the form given in [1]

$$n(t) = n_o \exp\left[-\frac{t}{\tau} - \gamma\sqrt{t} - \bar{W}t\right] \quad (5)$$

where $\gamma = (4/3)\pi^{3/2} N_a \sqrt{c_{\rm sa}}$ and

$$\bar{W} = \pi\left(\frac{2\pi}{3}\right)^{5/2} A_s R_{\rm sa}^3 R_{\rm ss}^3 N_s N_a \quad (6)$$

and exhibits a characteristic nonexponential decay (see Fig. 3). The diffusion model predicts the decay more accurately.

A. Transfer Efficiency

The energy-transfer efficiency between the sensitizer and the activator ions can be calculated by considering the lifetime for the energy manifold of the sensitizer involved in the transfer process. In a singly doped host material such as Yb:YCOB, the only de-excitation channels are radiative fluorescence or nonradiative decay to the ground state. In the codoped Er,Yb:YCOB

TABLE I
COMPARISON OF ENERGY TRANSFER PARAMETERS IN Er, Yb^{3+} CODOPED LASER HOSTS

Host	Phosphate Glass	YLF	YAG	YCOB
Er^{3+} Concentration, ($\times 10^{20}$ ions/cm^3)	2.0	1.4	1.4	0.88
Yb^{3+} Concentration , ($\times 10^{20}$ ions/cm^3)	4.0	14.0	9.0	8.8
Yb-Yb Migration co-eff, ($\times 10^{-39}$ cm^6/s)	-	19.0	1.0	8.45
Yb-Er Micro-parameter, ($\times 10^{-39}$ cm^6/s)	-	4.1	0.55	2.69
Er^{3+} Upconversion co-eff, ($\times 10^{-18}$ cm^3/s)	1.1	30.0	2.5	13.0
Yb-Er energy transfer rate, ($\times 10^3$ s^{-1})	8.0	0.3	2.1	12.9
Yb-Er critical interaction distance, (Å)	13.9 [1]	16	10	7.7
Concentration-dependent transfer rate, ($1/N_a$) ($\times 10^{-18}$ cm^{3}s^{-1})	40	2.1	15	130
Ref	[2]	[3]	[4]	This work

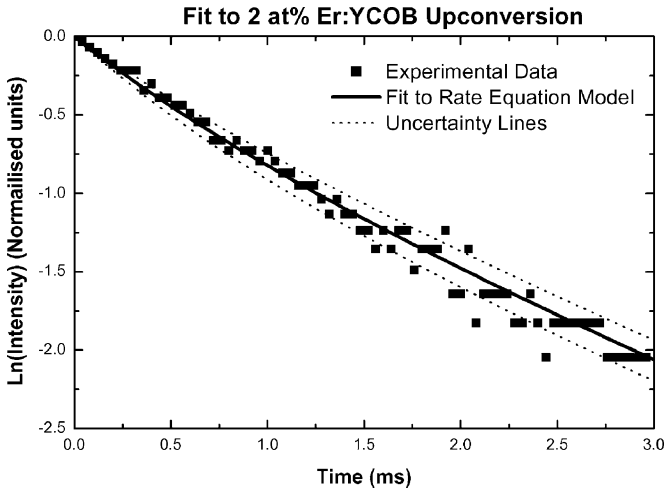

Fig. 2. Fit of the $^4I_{13/2}$ population decay in 2 at.% Er:YCOB to (A4) with upconversion parameters of $W_{\rm UC} = 1.30 \times 10^{-17}$ s^{-1}. The dotted lines indicate $\pm 0.4 \times 10^{-17}$ s^{-1} uncertainty margins.

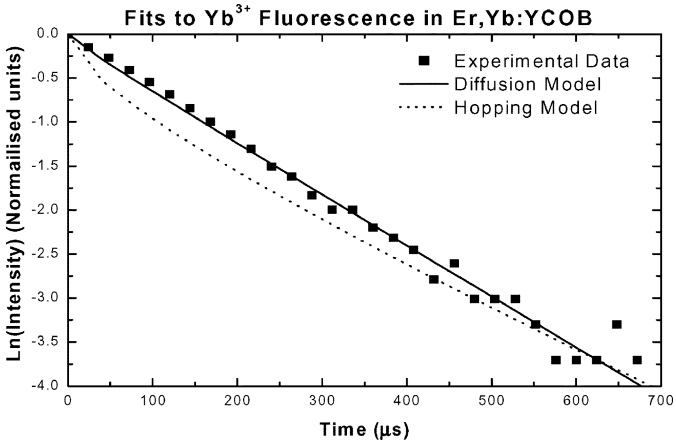

Fig. 3. Fits of the fluorescence decay of the Yb^{3+} $^2F_{5/2}$ manifold in the Er,Yb:YCOB crystal to the characteristic decay of the diffusion and hopping models.

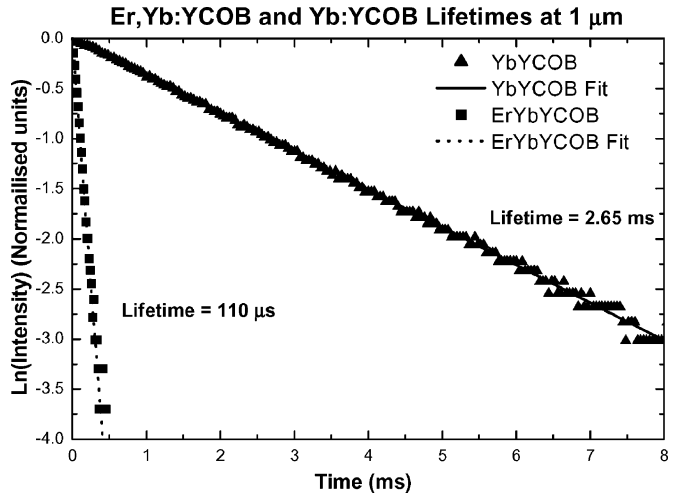

Fig. 4. Comparison between the lifetimes of the $^2F_{5/2}$ manifold of the Yb^{3+} sensitizer ions in the singly doped Yb:YCOB, and the codoped Er,Yb:YCOB.

host, however, resonant energy transfer further reduces the radiative lifetime of the sensitizer. Fig. 4 shows that the lifetime of the Yb^{3+} ions is reduced from 2.65 ms in the singly doped crystal to only 110 μs in the codoped crystal.

This transfer efficiency can be quantified by

$$\eta_{\rm ET} = 1 - \frac{\tau_s}{\tau_s^o} \tag{7}$$

where τ_s is the lifetime of the sensitizer in the codoped material and τ_s^o is the lifetime in the singly doped host. For the 2 at.% Er, 20 at.% Yb^{3+} YCOB crystal, the transfer is extremely efficient at $\eta_{\rm ET} \approx 96\%$. This compares well with other host materials.

IV. RATE-EQUATION ANALYSIS

The steady-state characteristics of the laser have been modeled using rate equations describing the rate of change with time of the populations of each electronic manifold involved in the laser system. Fig. 5 shows the energy level diagram of an Er,Yb system including key energy-transfer ($W_{\rm sa}$) and upconversion ($W_{\rm UC}$) channels. These two concentration-dependent processes are critical to the performance of the laser.

An increase in the Yb^{3+} concentration results in an increased absorption coefficient, which gives a larger population in the $^2F_{5/2}$ manifold (N_b) and, hence, an increased possibility of energy transfer. An increase in the Er^{3+} concentration also increases the energy transfer since more ions are available to be

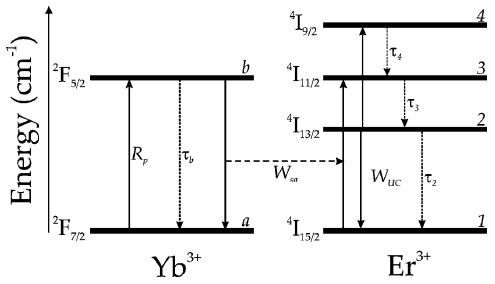

Fig. 5. Level assignment diagram and relevant processes for rate equation analysis of the Er,Yb:YCOB laser material.

excited. Conversely, increasing the Er^{3+} concentration also increases losses from the upper laser level due to nonradiative upconversion.

A. Er^{3+}, Yb^{3+}-Doped System

To model the population dynamics of the codoped Er,Yb system we use the set of rate equations shown in (8) and solve for steady-state conditions (CW pumping) with depletion of the Er^{3+} ground state included in the model. The Appendix gives the model for the crystal doped only with Er^{3+}

$$\frac{\partial N_b}{\partial t} = -\frac{\partial N_a}{\partial t} = R_p - \frac{N_b}{\tau_b} - W_{\rm sa}N_bN_1 + W_{\rm BT}N_aN_3 = 0 \quad (8a)$$

$$\frac{\partial N_1}{\partial t} = W_{\rm BT}N_aN_3 - W_{\rm sa}N_bN_1 + \frac{N_2}{\tau_2} + \beta_{31}\frac{N_3}{\tau_3} + \beta_{41}\frac{N_4}{\tau_4} + W_{\rm UC}N_2^2 = 0 \quad (8b)$$

$$\frac{\partial N_2}{\partial t} = \beta_{31}\frac{N_3}{\tau_3} - \frac{N_2}{\tau_2} + \beta_{42}\frac{N_4}{\tau_4} - 2W_{\rm UC}N_2^2 = 0 \quad (8c)$$

$$\frac{\partial N_3}{\partial t} = \beta_{43}\frac{N_4}{\tau_4} - \frac{N_3}{\tau_3} + W_{\rm sa}N_bN_1 - W_{\rm BT}N_aN_3 = 0 \quad (8d)$$

$$\frac{\partial N_4}{\partial t} = W_{\rm UC}N_2^2 - \frac{N_4}{\tau_4} = 0 \quad (8e)$$

$$N_{Yb} = N_a + N_b \quad (8f)$$

$$N_{Er} = N_1 + N_2 + N_3 + N_4. \quad (8g)$$

The levels designated by N_a, N_b, and N_{1-4} are shown in Fig. 5. The parameters τ_i are the lifetimes of the i-levels and the parameters β_{ij} are the branching ratios for transitions from the ith to jth levels. $W_{\rm UC}$ is the upconversion rate and $W_{\rm BT}$ is the back-transfer rate. R_p is the pump rate to the $\mathrm{Yb}(^2F_{5/2})$ level from the $\mathrm{Yb}(^2F_{7/2})$ ground state. The corresponding absorption from the Er^{3+} ground state is neglected since the Yb^{3+} concentration is an order of magnitude higher. The Er^{3+} pumping is due to energy transfer from Yb^{3+} to Er^{3+} via the process described by

$$W_{\rm sa} = \mathrm{Yb}(^2F_{5/2}) + \mathrm{Er}(^4I_{15/2}) \rightarrow \mathrm{Yb}(^2F_{7/2}) + \mathrm{Er}(^4I_{11/2}{}^4\mathrm{I}_{11/2}).$$

The model can be simplified by noting that the back-transfer parameter $W_{\rm BT}$ corresponding to $\mathrm{Yb}(^2F_{7/2}) + \mathrm{ER}(^4I_{11/2}) \rightarrow \mathrm{Yb}(^2F_{5/2}) + \mathrm{Er}(^4I_{15/2})$ is negligible due to the rapid depopulation of the resonant level $\mathrm{Er}(^4I_{11/2}) \rightarrow \mathrm{Er}(^4I_{13/2})$. Bleaching of the ground state manifolds is included in this model in that the N_1 and N_a manifolds can approach zero population as a result of large pump rates. This allows the opportunity to determine the level populations at realistic pump levels of a watt or more.

The emission rates of the Yb: $^2F_{5/2} \rightarrow {}^2F_{7/2}$ $(R_{\rm ba})$ and the Er: $^4I_{11/2} \rightarrow {}^4I_{15/2}$ (R_{31}) transitions are given by

$$R_{\rm ba} = \frac{N_b}{\tau_b}, \quad R_{31} = \beta_{31}\frac{N_3}{\tau_3}. \quad (9)$$

The ratio $q = R_{31}/R_{\rm ba}$ can be determined experimentally by comparing the fluorescence spectra for the Er:YCOB and the Yb:YCOB at 1 μm [3]. The emission rates are calculated by integrating the respective emission spectra, and q is an indication of the amount of overlap between the two. For the 2 at.% Er^{3+}, 2- at.% Yb^{3+}:YCOB crystal, the ratio of the emission rates was found to be $q = 0.2045 \pm 5\%$. The uncertainty arises from inherent uncertainties in the fluorescence collection method, and the weak Er^{3+} fluorescence in this region. This value of the overlap is higher than that for the Er^{3+}, Yb^{3+}:YLF crystal, [3].

Using the emission ratios in (9), the transfer parameters from (8a), (8b), and (8d) are eliminated, to yield a closed, analytical system for the population densities for the manifolds considered under steady-state pumping conditions.

If we consider a pump beam of 1.5 W incident onto the crystal with an Yb-ion absorption coefficient of $\alpha = 8\ \mathrm{cm}^{-1}$, and a spot size of 50 μm to give a pumping rate $R_p = 2.8407 \times 10^{23}$ ions $\mathrm{cm}^{-3}\mathrm{s}^{-1}$ and with an upconversion rate of $W_{\rm UC} = 1.30 \times 10^{-17}\ \mathrm{cm}^3/\mathrm{s}$, steady-state population densities of the 2 at.% Er^{3+}, 20 at.% Yb^{3+}:YCOB crystal are given in (10).

The analytical model was checked with the results of [3] using the stated constants for the YLF crystal host, and gave excellent agreement

$$\begin{aligned} N_{Yb} &= 8.99 \times 10^{20}\ \mathrm{cm}^{-3} & N_{Er} &= 8.99 \times 10^{19}\ \mathrm{cm}^{-3} \\ N_a &= 8.49 \times 10^{20}\ \mathrm{cm}^{-3} & N_1 &= 3.50 \times 10^{19}\ \mathrm{cm}^{-3} \\ N_b &= 4.98 \times 10^{19}\ \mathrm{cm}^{-3} & N_2 &= 5.49 \times 10^{19}\ \mathrm{cm}^{-3} \\ N_3 &= 3.25 \times 10^{15}\ \mathrm{cm}^{-3} & & \\ N_4 &= 3.35 \times 10^{14}\ \mathrm{cm}^{-3}. & & \end{aligned} \quad (10)$$

B. Population Inversion Characteristics of Er,Yb:YCOB

The simplest requirement for the operation of a laser is a population inversion between the upper and lower laser levels. The ability to maintain this population inversion under steady-state conditions at or near room temperature is a requirement for continuous-wave operation of the laser. However, the upper-lying Stark-split energy levels in each manifold have a finite population, described by the relation

$$f = \frac{1}{Z}\exp\left(\frac{-\Delta E}{kT}\right) \quad (11)$$

where ΔE is the energy difference between the level of interest and the lowest level of the manifold, k is the Boltzmann constant, T is the temperature of the crystal, and Z is the partition function of the manifold given by

$$Z = \sum_{i=1}^{n} g_i \exp\left[\frac{-E_i}{kT}\right] \quad (12)$$

TABLE II
STARK ENERGY LEVELS OF ER,YB:YCOB

Crystal	Manifold	Stark Energy Levels (cm^{-1})								
Yb:YCOB	$^2F_{5/2}$	10243	10618	11106						
	$^2F_{7/2}$	0	483	598	757	1061				
Er:YCOB	$^4F_{9/2}$	15060	15129	15313	15408	15480				
	$^4I_{9/2}$	12500	12591	12615						
	$^4I_{11/2}$	10169	10257	10364	10390					
	$^4I_{13/2}$	6394	6472	6502	6518	6566	6597	6644	6757	6881
	$^4I_{15/2}$	0	38	51	81	126	162	242	300	

where n is the number of distinct energy levels E_i in the manifold of interest and g_i is the degeneracy of the ith level.

To accurately determine the population inversion, we must consider the Stark levels involved in the stimulated emission process which have been determined by low-temperature absorption and emission experiments and the energy levels are given in Table II. The low-temperature emission spectrum of the erbium ion in YCOB shows a peak transition at a wavelength of $\sim$ 1555 nm between the lowest Stark level in the $^4I_{13/2}$ manifold, to about three closely spaced and thermally broadened levels 30–80 cm^{-1} above the ground level. Using (11) and (12), the fraction of the total number of atoms in a manifold that reside in the Stark level of interest can be determined. For the upper laser level, the fraction is calculated to be $f_{\text{upper}} = 0.476$ (or 41.6%) and the combination of lower laser levels to be $f_{\text{lower}} = 0.476$ at room temperature ($\sim$ 20 °C).

The population inversion characteristics of the erbium system between the upper laser level (the Er^{3+} $^4I_{13/2}$ manifold) and the ground state level (the Er^{3+} $^4I_{15/2}$ manifold) were modeled as a function of the Er^{3+} concentration on the crystal. Note that a population inversion does exist between these two levels for the 2 at.% Er^{3+}, 20 at.% Yb^{3+}:YCOB crystal for the pump rate used, sufficient for efficient laser operation.

C. Optimization of Concentration Ratios

To find the optimal Er^{3+}–Yb^{3+} dopant concentrations, the rate equation model of the codoped system was used to predict the expected population inversion for a range of Er^{3+} and Yb^{3+} concentrations. This removes the need for many samples to be grown with varying dopant concentrations and ratios.

Some approximations must be made. The decay rate of the Yb^{3+} ions caused by energy transfer to the Er^{3+} ions is approximated by an exponential fall-off with respect to the Er^{3+} concentration after the analysis of Philipps [1] for fluoride phosphate glasses. The relation was determined by fitting an exponential curve between the lifetime of the singly doped Yb:YCOB sample and the codoped sample. The upconversion rate increases with Er^{3+} concentration, and this was approximated by a linear function after the analysis of Er,Yb-doped phosphate glasses by Hwang [2] who found that the upconversion rate was constant with respect to the

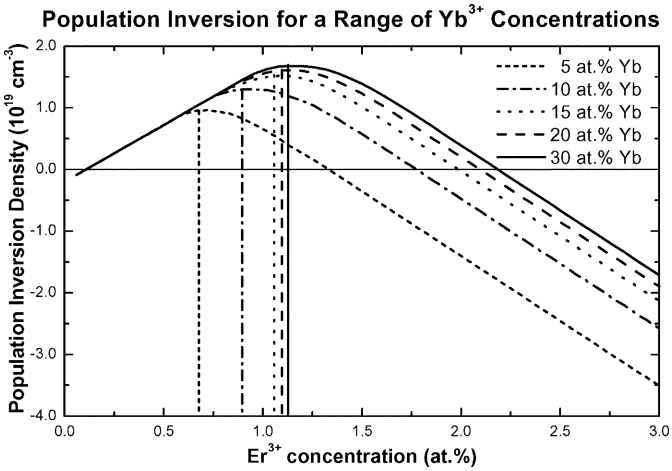

Fig. 6. Population inversion densities ($N_{\text{upper}} - N_{\text{lower}}$) in Er^{3+} for a range of Yb^{3+} concentrations. The optimum Er^{3+} concentration (ie. at the maximum inversion) is marked.

Yb^{3+} concentration. [19] studied the dynamics of Er,Yb-doped lithium niobate ($LiNbO_3$) crystals and found that the lifetime of the Er^{3+} $^4I_{13/2}$ manifold was not affected by the Yb^{3+} concentration and so remains as a constant in the analysis. They also found that the lifetime of the Yb^{3+} $^2F_{5/2}$ manifold increased slightly with increasing Yb^{3+} concentration, but this has been neglected here.

The Boltzmann population of the upper and lower Stark laser levels were calculated from the fractional populations of the total manifold populations. A population inversion (i.e., $N_{\text{upper}} - N_{\text{lower}} > 0$) exists up to an Er^{3+} concentration of approximately 2 at.%. The optimum Er^{3+} concentrations for the Yb^{3+} concentrations evaluated are shown in Fig. 6. The pump rate for all these figures has been calculated assuming an incident pump power of $P_{\text{in}} = 1.5$ W, resulting in a rate of 3.05×10^{23} photons/s. Using the results from Fig. 6, crystals with the desired dopant concentrations were grown resulting in crystals with Yb^{3+} concentration of 30 at.% and Er^{3+} concentration of 1.4 at.%, verified by inductively coupled-plasma mass spectroscopy (ICPMS) analysis. Further, the upconversion coefficient and the lifetime of the Yb^{3+} ions were calculated in the same way as before, and compared well with the experimental values. While the new laser crystal dopant concentrations were

not quite optimum, we should expect greatly improved laser operation.

V. CW Laser Output

A. Experimental Details

The crystal used was a Y-cut 2-mm-long Er,Yb:YCOB with one face coated for high-reflection (HR) ($\mathrm{R} > 99\%$) between 1.4 and 1.6 μm and high transmission ($\mathrm{T} \approx 92\%$) at 975 nm. The output face was anti-reflection (AR) coated ($\mathrm{R} < 0.5\%$) between 1.4–1.6 μm. The pump source was an optical fiber coupled laser diode with a 50-μm diameter core and a numerical aperture N.A. = 0.22. The maximum output power was 2.8 W at 975 nm, giving an M^2 factor of 17.9 and a brightness at the face of the fiber of $\sim$1280 kW/cm^2. Output from the fiber was first collimated and then refocussed into the laser crystal by moulded glass aspheric lenses.

The focused pump spot size was $\sim$ 115 μm diameter. About 90% of the maximum output from the pump fiber was incident on the laser crystal. The absorption coefficient at 976 nm due to the Yb^{3+} ions was $\alpha = 12\ \mathrm{cm}^{-1}$, resulting in $\sim$ 91% absorption of the pump light in the crystal.

The disadvantage of this pump source was that the output spectrum had a fluctuating bandwidth of $\sim$ 6–8 nm. Since the bandwidth of the Yb:YCOB absorption feature at 976 nm is only approximately 4 nm, only $\sim$ 65% of the available pump radiation was absorbed in the crystal. The crystal was mounted carefully with indium foil to maintain thermal conduction.

The laser crystal was set up in both a hemispherical cavity with a 200-mm radius of curvature output (RoC) coupler, and a flat-flat cavity. The output coupling in both cases was 1%.

B. Laser Output

The output characteristics of the laser are shown in Fig. 7. 255 mW of CW laser radiation at 1.55 μm was obtained in the hemispherical cavity and 164 mW CW with the flat-flat cavity configuration. This is a significant improvement of 2.5 times over previous results, due to the fact that more power is available, at sufficient brightness to achieve population inversion. The slope efficiencies were 26.8% and 21.5% for the hemispherical and flat-flat cavities, respectively. The threshold of the hemispherical cavity laser $\sim$ 800 mW compares favorably with predictions based on standard laser models [20], [21] and described in detail in [22]. This result shows that Er,Yb:YCOB lasers are comparable to the most efficient laser output attained with the Er,Yb-doped phosphate bulk glass laser hosts, namely CW multimode 1.55-μm laser output of 320 mW with a slope efficiency of 27% [23]. Note that the phosphate glass laser hosts have been pursued as the laser host of choice for the past ten years or more, whereas the YCOB host has been under development for less than three years.

C. Output Spectra

The free-running emission spectrum of the 1.55-μm output in the flat-flat cavity can be seen in Fig. 8, which is an accumulation of seven individual scans. Coupled-cavity effects [24] are evident in the spectrum with closely spaced longitudinal modes separated into mode groups approximately 1.8 nm apart.

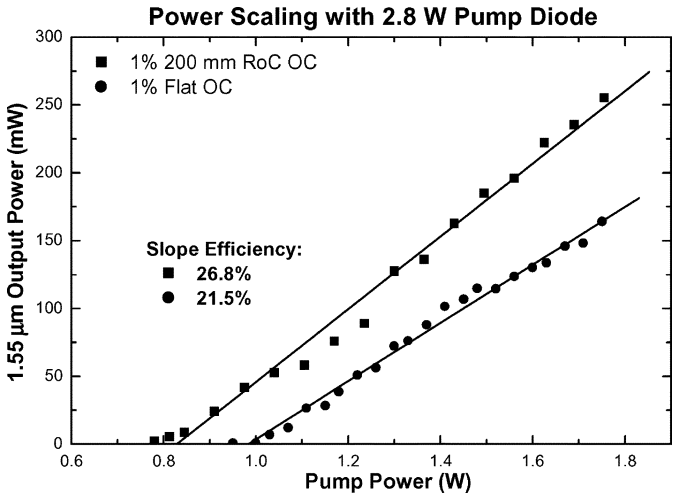

Fig. 7. Er,Yb:YCOB laser output using the 2.8 W fiber coupled diode pump laser. The maximum output was $\sim$ 250 mW of CW radiation.

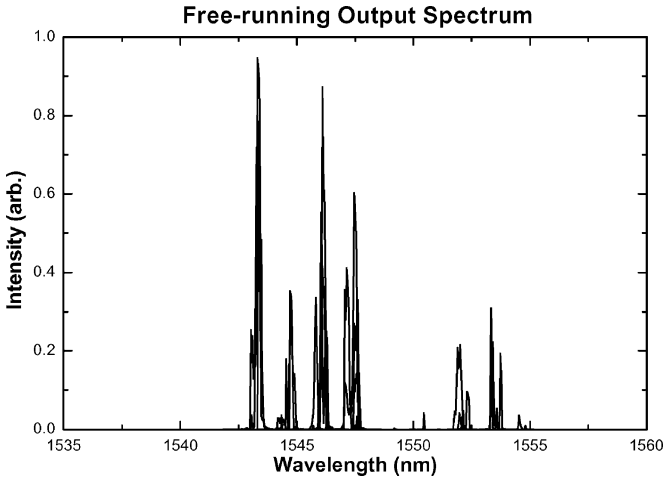

Fig. 8. Free-running output spectrum of the Er,Yb:YCOB laser in the flat-flat cavity configuration. Spectrum is the accumulation of seven individual wavelength scans.

D. Amplitude and Temperature Stability

The stability of the laser output is demonstrated in Fig. 9. The long-term stability at 110 mW was measured by detecting the output with a p-i-n photodiode over 10 min. The power amplitude variation is described by twice the standard deviation (σ) divided by the average power and is found to be $\sim$ 1.2%. The variation of the output power with respect to crystal mount temperature (Fig. 10) is found to be only -0.3 mW/ °C indicating that the laser is operating as a quasi-four-level laser.

VI. Conclusion

Optimum dopant concentrations have been calculated and efficient laser operation of an Er,Yb-doped YCOB crystal has been demonstrated. Multilongitudinal-mode output of 250 mW has been obtained with a slope efficiency of $\sim$ 27%, which is comparable to the best CW result to date achieved in the phosphate glass host. 150 mW of output has also been achieved with a plano/plano cavity. Significant improvement is expected in the hemispherical cavity with OCs of shorter RoC ($\sim$ 25 mm) which

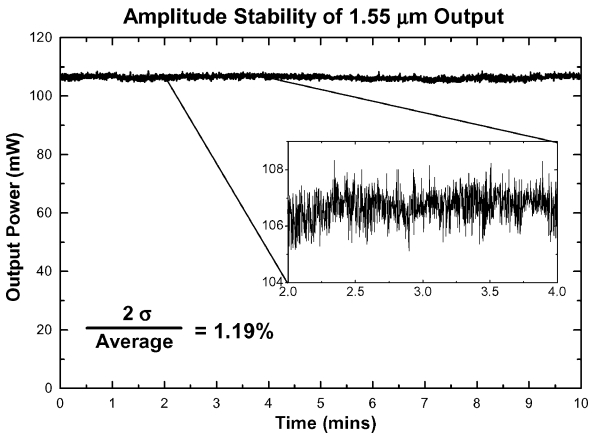

Fig. 9. Amplitude stability of 1.55-μm laser output at maximum power (1% 200 mm OC).

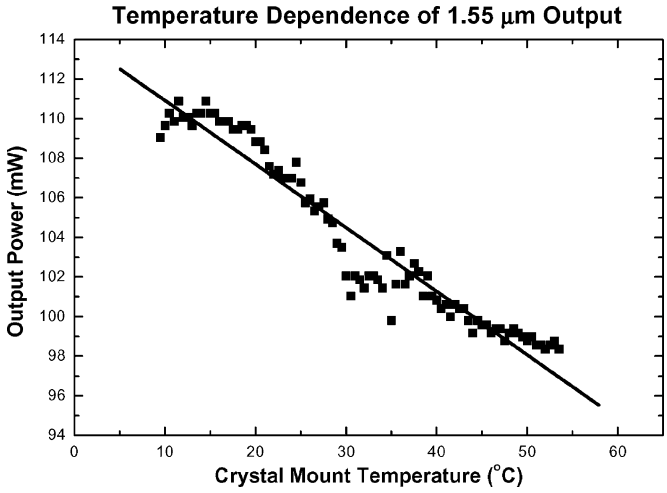

Fig. 10. Temperature dependence of laser output (1% 200 mm OC). The degradation of output power with temperature is -0.3 mW/°C.

will improve the pump-to-laser mode matching efficiency. Good long-term amplitude stability and relative insensitivity to temperature variations of the crystal mount have been established at power levels of greater than 100 mW.

APPENDIX
Er^{3+}-DOPED SYSTEM

The rate equations for a singly doped Er^{3+} laser system can be written as

$$\frac{\partial N_1}{\partial t} = -R_p + \frac{N_2}{\tau_2} + \beta_{31}\frac{N_3}{\tau_3} + \beta_{41}\frac{N_4}{\tau_4} = 0 \quad \text{(A1a)}$$

$$\frac{\partial N_2}{\partial t} = \beta_{31}\frac{N_3}{\tau_3} - \frac{N_2}{\tau_2} + \beta_{42}\frac{N_4}{\tau_4} - 2W_{\rm UC}N_2^2 = 0 \quad \text{(A1b)}$$

$$\frac{\partial N_3}{\partial t} = R_p + \beta_{43}\frac{N_4}{\tau_4} - \frac{N_3}{\tau_3} = 0 \quad \text{(A1c)}$$

$$\frac{\partial N_4}{\partial t} = W_{\rm UC}N_2^2 - \frac{N_4}{\tau_4} = 0 \quad \text{(A1d)}$$

$$N_{Er} = N_1 + N_2 + N_3 + N_4 \quad \text{(A1e)}$$

where N_i $(i = 1 - 4)$ are the populations in each of the energy manifolds defined in Fig. 5, and N_{Er} is the concentration of Er^{3+} in the crystal in units of ions/cm^3. Using the steady-state assumption, the rate of change of the populations has been set to zero. See main text for a definition of the parameters. It is clear from (A1b) that upconversion is a significant loss mechanism since each event removes two excited ions from the upper laser level, and the probability is proportional to the square of population N_2. R_p is the pump rate to the $^4I_{11/2}$ level assuming a pump wavelength of 980 nm. This is calculated from

$$R_p = \frac{\lambda_p}{hc}\frac{1}{d\pi\omega^2}[1 - \exp(-\alpha(\lambda_p)d)]P_{in} \quad \text{(A2)}$$

where λ_p is the pump wavelength, h is Planck's constant, d is the length of the crystal, ω is the radius of the pump spot in the crystal, $\alpha(\lambda_p)$ is the absorption coefficient at the pump wavelength, and P_{in} is the pump power incident on the crystal.

Because of the small energy gaps between the $^4I_{11/2}$ and $^4I_{13/2}$ levels, and between the $^4I_{9/2}$ and $^4I_{11/2}$ levels, in comparison with the large phonon energy of the YCOB host, decay from the $^4I_{11/2}$ and $^4I_{9/2}$ levels is dominated by fast nonradiative transitions. These transition rates are many orders of magnitude faster than the pump rate R_p, hence, the populations N_3 and N_4, respectively, in these levels are negligible. This is confirmed by calculation of the steady-state populations with a known pump rate and measured decay parameters. The maximum populations observed in the $^4I_{11/2}$ and $^4I_{9/2}$ levels are less than 0.15% and 10 $^{-4}$% of the total Er^{3+} concentration, even for large pump powers (up to 1.5 W). Taking this into account, the rate equations can be simplified to

$$\frac{\partial N_2}{\partial t} = -\frac{\partial N_1}{\partial t} = R_p - \frac{N_2}{\tau_2} - W_{\rm UC}N_2^2 = 0 \quad \text{(A3a)}$$

$$N_{\rm Er} = N_1 + N_2. \quad \text{(A3b)}$$

When the lifetime is measured under weak excitation, the population N_2 is small and the quadratic upconversion term can be neglected. The decay of the excited level then becomes a single exponential with lifetime τ_2^o. When the pump power is increased, the upconversion needs to be considered and can be solved from (A3) as

$$N_2(t) = \frac{1}{\tau_2^o}\frac{1}{\left(\frac{1}{\tau_2^o N_2(0)} + W_{\rm UC}\right)\exp\left[\frac{t}{\tau_2^o}\right] - W_{\rm UC}} \quad \text{(A4)}$$

where $N_2(0)$ is the steady-state population at $t = 0$ (when the pump is switched off), and depends on the pump power. The only unknown parameter is $W_{\rm UC}$, which can be found by fitting the luminescence decay curves with (A4). This is demonstrated for Er:YCOB above. The upconversion coefficient in Er^{3+} samples cosensitised with Yb^{3+} is assumed consistent with that observed in an Er^{3+}-doped sample with the same Er^{3+} concentration [2].

REFERENCES

[1] J. F. Philipps, T. Töpfer, H. Ebendorff-Heidepriem, D. Ehrt, and R. Sauerbrey, "Spectroscopic and lasing properties of Er^{3+}:Yb^{3+}-doped fluoride phosphate glasses," *Appl. Phys. B, Lasers Opt.*, vol. 72, pp. 399–405, 2001.

[2] B.-C. Hwang, S. Jiang, T. Luo, J. Watson, Sorbello, and N. Peyghambarian, "Cooperative upconversion and energy transfer of new high Er^{3+}- and Yb^{3+}-Er^{3+}-doped phosphate glasses," *J. Opt. Soc. Amer. B*, vol. 17, pp. 833–839, 2000.

[3] C. Wyss, W. Luthy, H. P. Weber, P. Rogin, and J. Hullinger, "Energy transfer in Yb^{3+}:Er^{3+}:YLF," *Opt. Commun.*, vol. 144, pp. 31–35, 1997.

[4] P. Lacovara, "Energy transfer and upconversion in Yb:YAG and Yb:Er:YAG," P.hD. dissertation, Boston College, Chestnut Hill, MA, 1992.
[5] J. T. Vega-Duran, O. Barbosa-Garcia, L. A. Diaz-Torres, M. A. Meneses-Nava, and D. S. Sumida, "Effects of energy back transfer on the luminescence of Yb and Er ions in YAG," *Appl. Phys. Lett.*, vol. 76, pp. 2032–2034, 2000.
[6] R. E. Di Paolo, E. Cantelar, X. M. Wang, T. Tsuboi, and F. Cusso, "Determination of the Er^{3+} to Yb^{3+} energy transfer efficiency in Er^{3+}/Yb^{3+}-codoped YVO_4 crystals," *J. Phys.: Condensed Matter*, vol. 13, pp. 7999–8006, 2001.
[7] L. Zhang, H. Hu, C. Qi, and F. Lin, "Spectroscopic properties and energy transfer in Yb^{3+}/Er^{3+}-doped phosphate glasses," *Opt. Mat.*, vol. 17, pp. 371–377, 2001.
[8] L. Laversenne, S. Kairouani, Y. Guyot, C. Goutaudier, G. Boulon, and M. T. Cohen-Adad, "Correlation between dopant content and excited-state dynamics properties in Er^{3+}-Yb^{3+}-codoped Y_2O_3 by using a new combinatorial method," *Opt. Mat.*, vol. 19, pp. 59–66, 2002.
[9] T. Forster, "Intermolecular energy migration and fluorescence," *Annal. Phys.*, vol. 6, pp. 55–75, 1948. Translated by R. S. Knox, Univ. Rochester, 1974, 1984.
[10] D. L. Dexter, "A theory of sensitized luminescence in solids," *J. Chem. Phys.*, vol. 21, pp. 836–850, 1953.
[11] A. I. Burshtein, "Hopping mechanism of energy transfer," *Sov. Phys.—JETP* , vol. 35, pp. 882–885, 1972.
[12] N. Bloembergen, *Physica*, vol. 15, pp. 386–426, 1949.
[13] A. M. Tkachuk and S. I. Klokishner, "Self-quenching of luminescence of rare-earth ion in crystals," *Opt. Spectrosc.* , vol. 61, pp. 55–59, 1985.
[14] R. C. Powell, *Physics of Solid-State Laser Materials*. New York: Springer-Verlag, 1998.
[15] D. L. Veasey, D. S. Funk, P. M. Peters, N. A. Sanford, G. E. Obarski, N. Fontaine, M. Young, A. P. Peskin, W.-C. Liu, S. N. Houde-Walter, and J. S. Hayden, "Yb/Er-codoped and Yb-doped waveguide lasers in phosphate glass," *J. Non-Cryst. Solids*, vol. 263-264, pp. 369–381, 2000.
[16] H. Zhang, X. Meng, C. Wang, P. Wang, L. Zhu, X. Liu, C. Dong, Y. Yang, R. Cheng, J. Dawes, J. Piper, S. Zhang, and L. Sun, "Growth, spectroscopic properties and laser output of $Er:Ca_4YO(BO_3)_3$ and $Er:Yb:CA_4YOBO_3)_3$ crystals," *J. Cryst. Growth*, vol. 218, pp. 81–86, 2000.
[17] P. Wang, J. M. Dawes, P. Burns, J. A. Piper, H. Zhang, L. Zhu, and X. Meng, "Spectral characterization of Er^{3+}:Yb^{3+}:YCOB crystals at 1.5–1.6 μm," *OSA TOPS*, vol. 34, pp. 207–211, 2000.
[18] M. Yokota and O. Tanimoto, "Effects of diffusion on energy transfer by resonance," *J. Phys. Soc. Jpn.*, vol. 22, pp. 779–784, 1967.
[19] E. Cantelar and F. Cuss'o, "Dynamics of the Yb^{3+} to Er^{3+} energy transfer in $LiNbO_3$," *Appl.Phys. B, Laser Opt.*, vol. 69, pp. 29–33, 1999.
[20] T. Taira, W. M. Tulloch, and R. L. Byer, "Modeling and quasithree-level lasers and operation of CW Yb:YAG lasers," *Appl. Opt.*, vol. 36, pp. 1867–1874, 1997.
[21] P. Laporta, S. Longhi, S. Taccheo, and O. Svelto, "Analysis and modeling of the erbium-ytterbium glass laser," *Opt. Commun.*, vol. 100, pp. 311–321, 1993.
[22] P. A. Burns, "Novel miniature laser sources based on ytterbium doped crystals," Ph.D. dissertation, Maqcuarie Univ., Sydney, Australia, 2003.
[23] S. Taccheo, G. Sorbello, P. Laporta, G. Karlsson, and F. Laurell, "230-mW diode-pumped single-frequency Er:Yb laser at 1.5 μm," *IEEE Photon. Technol. Lett.*, vol. 13, pp. 19–21, 2001.
[24] C. Pedersen, P. L. Hansen, T. Skettrup, and P. Buchave, "Diode-pumped single-frequency $Nd:YVO_4$ laser with a set of coupled resonators," *Opt. Lett.*, vol. 20, pp. 1389–1391, 1995.

Phillip A. Burns (M'00) received the B.Tech. (hons.) and Ph.D. degrees from Macquarie University, Sydney, Australia, in 2000 and 2004, respectively.

His research interests while at Macquarie University concerned diode-pumped solid-state lasers. He has since moved away from research and has taken a position as a patent attorney with Shelston IP, Sydney, Australia.

Judith M. Dawes received the B.Sc. (hons.) and the Ph.D. degrees from Sydney University, Sydney, Australia, in 1989.

After postdoctoral research at the University of Toronto, Toronto, ON, Canada, she joined the Centre for Lasers and Applications, Department of Physics, Macquarie University, Sydney. She is currently an Associate Professor of Physics at Macquarie University, with research interests in the physics of solid-state lasers, nonlinear optical laser crystals, tunable lasers, and laser applications in medicine.

Peter Dekker received the B.Sc. and M.Sc. (hons.) degrees from Macquarie University. Sydney, Australia, in 1988 and 1998, respectively. He is currently pursuing the Ph.D. degree at Macquarie University, focusing on ytterbium solid-state lasers.

He is currently a Professional Officer within the Centre for Lasers and Applications, Department of Physics, Macquarie University. He has conducted research in various solid-state laser and nonlinear optical laser systems and medical applications of lasers.

James A. Piper received the B.Sc. (hons.) and Ph.D. degrees from Otago University, Dunedin, New Zealand, in 1968 and 1971, respectively.

After post-doctoral research at Oxford University, he has worked at Macquarie University, Sydney, Australia, since 1975, where he is a Professor of physics, foundation director of the Centre for Lasers and Applications, and currently Deputy Vice Chancellor for Research. He has conducted research in continuous-wave metal-ion lasers, cyclic pulsed metal-vapor lasers, recombination lasers, pulsed dye lasers, frequency conversion techniques for high-power gas lasers, diode-pumped solid-state lasers, solid-state Raman lasers, and laser applications in medicine and industry.

Dr. Piper has been awarded the Pawsey Medal by the Australian Institute of Physics and is a Fellow of the Australian Institute of Physics and of the Optical Society of America.

Huaidong Jiang received the Ph.D. degree from Shandong University, Jinan City, China, in 2003.

He is currently with the Department of Physics, National University of Singapore, Singapore.

Jiyang Wang received the Ph.D. degree from Nanjing University, Nanjing, China, in 1968.

He worked at Bowling Green State University, Bowling Green, OH, from 1994 to 1998 and the University of Koln, Koln, Germany, from 1984 to 1986 and from 1990 to 1991. He is currently Professor, Deputy Director of the State Key Laboratory of Crystal Materials, and Director of the Institute of Crystal Materials, Shandong University, Shandong, China, where his research interests include growth and characterization of functional crystals, mainly nonlinear optical and laser crystals.

Dr. Wang has been awarded the Science and Technology Progress Award (1994) and the National Invention Award (1996) in China.